Six-mode Scrambler based on Cascaded Side-Wall Grating Waveguides

Takeshi Fujisawa,[1*] Taiji Sakamoto,[2] Masashi Miyata,[3] Takashi Matsui,[2] Toshikazu Hashimoto,[3] Ryoichi Kasahara,[3] Takayoshi Mori,[2] Ryota Imada,[2] Kazuhide Nakajima,[2] and Kunimasa Saitoh,[1]

[1]*Graduate school of Information Science and Technology, Hokkaido University, Sapporo, Hokkaido, 060-0814, Japan.*

[2]*NTT Access Network Service Systems Laboratories, NTT Corporation, Ibaraki 305-0805, Japan*

[3]*NTT Device Technology Laboratories, NTT Corporation, Kanagawa 243-0198, Japan*

E-mail: fujisawa@ist.hokudai.ac.jp

Abstract

A six-mode scrambler based on cascaded side-wall long-period-grating waveguides on silica planar lightwave circuit (PLC) platform is proposed for mode-division-multiplexing (MDM) transmission. The device can be fabricated with only one-step etching since it does not use a surface grating. A mode-dependent loss (MDL) of the system is estimated and the MDL can be reduced with multiple scrambling operation. Two gratings proposed here and a fiber-pigtailed module containing these gratings are fabricated and expected proof-of-concept mode scrambling operation is confirmed. It is found that the connection between few-mode fiber (FMF) and PLC chip seems to be the dominant loss of the module. Considering these losses, the measured results are in good agreement with the calculated results.

1. Introduction

A mode-division-multiplexing (MDM) technique has attracted a lot of attentions to increase the capacity of optical fiber transmission system. In MDM system, a multiple-input multiple-output (MIMO) technique is usually used to undo the mode mixing occurred in few-mode fiber (FMF) at the receiver. In MIMO processing, so-called differential mode delay (DMD) and mode-dependent loss (MDL) deteriorates the receiver performance. Too large DMD and MDL make it difficult to recover the signal[1-3].

To overcome these problems, a mode exchanging technique at a relay point between two FMFs is useful[4,5]. In [4,5], six-modes transmitted in FMF is demultiplexed to fundamental modes and multiplexed again with cyclically changed modes. The technique is useful to reduce total DMD. To install the mode exchanging unit to the transmission system, the device should be small, and therefore, an integrated type mode-exchanger (mode-EX) is preferable due to its small size and mass productivity. In mode-EX, various mode converting operations are necessary and many kinds of mode converting or exchanging devices have been proposed in several waveguide platforms, such as Si-photonics[6-10], polymer[11-13], and silica waveguides[14]. Among them, a long-period grating (LPG) waveguide is one of the promising candidates for mode exchanging devices. By properly designing the grating pitch, it is possible to exchange arbitrary two modes.

In [11,12], LPG-based mode converters were proposed for polymer waveguide platforms and successful mode conversion for three modes were demonstrated. However, to convert LP_{11a} and LP_{11b} modes separately, the sidewall and the surface gratings have to be formed, leading to difficult fabrication process. In [14], a cascaded directional coupler type three-mode-EX was demonstrated in silica planar lightwave circuit (PLC) platform. Although silica waveguides have some advantages, such as, low-loss connection to FMF and good reliability, the circuit was complex and it is difficult to increase the number of modes. Especially, six-mode operation is desired for 4 linearly polarized (LP) mode transmission. In [13], although the method of six-mode conversion was demonstrated based on polymer LPG with surface trench structure, it needs special photolithography mask for fabricating surface trench.

In the MIMO receiver, one of the important characteristics is a mode-dependent loss (MDL). If the MDL becomes small, a perfect cyclic mode conversion, shown in above

studies, is not always necessary, but, a mode scrambling technique[15-17], in which multiple modes are mixed with proper power ratio, might be also useful for reducing MDL. In [17], a six-mode mixer based on two cascaded long-period fiber grating (LPFG) was proposed and no MDL degradation originating from the device was demonstrated. However, the total size of two LPFGs was over 60 mm and the size reduction is preferable. For that purpose, an integrated type mode-scrambler is useful due to its small size and mass productivity.

In this paper, a six-mode scrambler based on cascaded side-wall LPG waveguides on silica PLC platform proposed in [18] is experimentally demonstrated for the first time. Two side-wall LPGs are designed and fabricated: one is for E_{11}-E_{12} and E_{21}-E_{22} mode conversions, and the other is for E_{11}-E_{31} mode conversion. By properly designing grating parameters, two mode sets can be simultaneously converted with one grating. An LP-mode-group scrambling operation, which is preferable for fiber based MDM transmission, is possible by cascading these two gratings together with adiabatic and short taper waveguides for E_{31},E_{13}-LP_{21b},LP_{02} mode conversion. Unlike previously reported LPG mode converters[11,12], the proposed device does not need the surface grating since E_{21}-E_{11} mode conversion is not used, leading to significantly simplified fabrication process. In addition to our preliminary conference report [18], detailed theoretical design and experimental results are added in this paper. Two gratings proposed here and a fiber-pigtailed module containing these gratings are fabricated. It is found that the connection between pigtailed-FMF and PLC chip seems to be the dominant loss of the module. Considering these losses, the measured results are in good agreement with the calculated results and expected mode-group scrambling operation is confirmed. It should be noted that the proposed device is not for “mode-group” transmission, but for usual MIMO-based MDM transmission.

2. Theoretical design

2.1 Overall structure and operation principle

Figure 1 (a) shows field distributions of six modes in rectangular waveguide. In these modes, E_{11}, E_{12}, E_{21}, and E_{22} modes can be viewed as LP_{01}, LP_{11a}, LP_{11b}, and LP_{21a} fiber modes. Although E_{13} and E_{31} modes are not like fiber modes, they can be converted to LP_{21b}- and LP_{02}-like modes as shown later. Therefore, we consider mode mixing of these six modes in rectangular waveguides. A sidewall or surface grating can be used for the mode

conversion between these modes. In the sidewall grating, the waveguide sidewall is corrugated, whereas the top surface of the waveguide is corrugated in the surface grating. The side-wall grating can convert the modes having different mode order in horizontal direction. The surface grating can convert the modes having different mode order in vertical direction. For the six-mode case, the allowable mode converting combinations are shown in Fig. 1(b). The side-wall grating can convert three combinations (E_{11}-E_{12}), (E_{21}-E_{22}), and (E_{11}-E_{31}). The top grating can convert two combinations (E_{11}-E_{12}), and (E_{11}-E_{13}). To achieve completely cyclic mode exchanging operation, both sidewall and top gratings have to be used. However, for a mode scrambling operation, the complete cyclic mode exchanging operation is not always necessary in terms of reducing MDL, as shown later. Also, our preliminary calculation indicates that the loss of E_{13} mode in the surface grating is relatively large leading to increased device MDL. Therefore, here, we only consider the sidewall gratings for the proposed six-mode scrambler to reduce MDL and ease the fabrication process.

Figure 1 (c) shows the schematic of the mode scrambler and LPG waveguide proposed here. Two kinds of gratings, G1 and G2 are concatenated together with taper waveguides at the input and output. Taper waveguides are used to convert fiber LP modes to rectangular waveguide modes. As shown in Fig. 1 (b), G1 converts two mode sets (E_{11}-E_{12} and E_{21}-E_{22}) simultaneously, because by properly optimizing the grating parameters, simultaneous mode conversion with only one grating is possible. G2 converts E_{11} mode to E_{31} mode. It should be noted that, in this configuration, (E_{11}, E_{21}, E_{31}, E_{13}) mode group and (E_{12}, E_{22}) mode group are separately mixed, as shown later in Fig. 7. However, in FMF transmission, degenerate modes (LP_{11a}, LP_{11b}) and (LP_{21a}, LP_{21b}) are easily mixed, and therefore, the six modes are fully mixed in total.

2.2 Grating and taper waveguide design

Here, we consider silica waveguide. The relative index difference between core and cladding is 1.1% and the thickness of the core is 10 μm. The waveguide width is W and LPG is formed on one side of the sidewall. The pitch, the depth, and the length of the grating waveguide are Λ, d, and L, respectively. The pitch of the grating for desired mode conversion can be obtained by

$$\Lambda = \frac{\lambda}{n_{eff,m} - n_{eff,n}} \quad (1)$$

where $n_{\mathrm{eff,m}}$ is the effective refractive index of the m-th mode, and the wavelength λ = 1.55 μm. For the design of LPGs, we first calculate the grating pitch by equation (1) using mode-solver based on a finite-element method (FEM). And then, the transmission characteristics are calculated using a beam propagation method (BPM)[19] by changing d and L. We optimize the grating geometry to maximize the modal conversion efficiency. Here, the modal conversion efficiency is defined as the transmitted power of the desired mode at the output of the device, which is directly calculated with the overlap integral between desired mode field and the field obtained by BPM. Since there are almost no polarization dependence, only quasi transverse electric (quasi-TE) modes are considered in this paper.

Here, two kinds of gratings are considered. Grating 1 (G1) converts two mode sets (E_{11}-E_{12} and E_{21}-E_{22}) simultaneously, because by properly optimizing the grating parameters, simultaneous mode conversion with only one grating is possible. Grating 2 (G2) converts E_{11} mode to E_{31} mode. d is set to 0.5 μm to reduce the scattering loss and the grating pitches are set to 440 and 170 μm for G1 and G2. The pitch for G1 is determined to convert two mode sets (E_{11}-E_{12} and E_{21}-E_{22}) simultaneously. Figures 3 (a) and (b) show E_{11}-E_{12} and E_{21}-E_{22} conversion spectra of G1 for different periods, N. By increasing N, the conversion efficiency is increased. The conversion peaks are around 1550 and 1590 nm for E_{11}-E_{12} and E_{21}-E_{22} conversions. To obtain large conversion efficiency for both conversions, we set N = 14 (total 6160 μm). Figure 3 (c) shows E_{11}-E_{31} conversion spectra of G2 for different periods. To obtain large conversion efficiency at 1550 nm, we set N = 23 (total 3910 μm). Table 1 shows the optimized grating parameters for W = 11 μm.

Figure 3 (a) shows calculated $|E_x|$ field distributions in xz-plane when E_{11} and E_{12} modes are launched to G1. In the proposed grating, since E_{12}-E_{22} mode conversion, which can be achieved by the sidewall grating is used, the fabrication process is significantly simplified. Figure 3 (b) shows calculated $|E_x|$ field distributions in xz-plane when E_{11} mode is launched to G2. Successful mode conversion to E_{31} mode can be seen.

Since we are interested in fiber-based MDM transmission, the guided mode should be LP-like mode rather than E_{pq} mode. E_{11}, E_{21}, E_{12}, and E_{22} modes can be viewed as LP_{01}, LP_{11a}, LP_{11b}, and LP_{21a} modes, respectively, as shown in Fig. 1 (a). However, E_{31} and E_{13} modes are

not like LP_{21b} and LP_{02} modes. Here, short and adiabatic taper waveguides[20] are used for converting E_{31} and E_{13} modes to LP_{21b}- and LP_{02}-like modes. In the square waveguide, there exist LP_{21b}- and LP_{02}-like modes as a hybrid mode of E_{31} and E_{13} modes. Figure 4 (a) shows the expected mode conversion in short and adiabatic taper waveguides. LP_{21b} and LP_{02} modes coming from FMF are converted to the mixture of E_{31} and E_{13} modes in the short taper due to the abrupt change in the waveguide width. On the other hand, in the adiabatic taper waveguide, E_{13} and E_{31} modes coming from the grating are converted to LP_{21b}- and LP_{02}-like modes without mode mixing, due to the adiabatic conversion. The length of short taper is 100 μm and modal output powers calculated by BPM are shown in Fig. 4 (b). There are almost no losses and LP_{21b} and LP_{02} modes are converted to E_{13} and E_{31} modes, almost equally. The adiabatic taper employs two-stage tapering[20] and the total length is 6000 μm. The waveguide widths at both sides are 10 (square cross section) and 11 μm.

Figure 5 (a) and (b) show the calculated 6×6 mode-group coupling matrices of G1 and G2 with taper waveguides. The row and column of the matrix correspond to input and output mode groups. The mode-group order is the same for row and column. In each row, the sum of the mode powers of the input mode is set to 0 dB. (LP_{01} - LP_{11a} and LP_{11b} - LP_{21a}) conversions for G1, and (LP_{01} - LP_{02}) conversion for G2, are seen. The MDL calculated from the singular values of complex transmission matrix[21] are 0.85 and 2.5 dB for G1 and G2, respectively. Here, the MDL is calculated as follows. The transmission matrix is defined as

$$\boldsymbol{\phi}_{out} = \boldsymbol{T}\boldsymbol{\phi}_{in} \tag{2}$$

where $\boldsymbol{\phi}_{in}$ is input mode vector and $\boldsymbol{\phi}_{out}$ is output mode vector. $\boldsymbol{T}$ is the complex transmission matrix calculated by BPM. Theoretical MDL (in dB unit) is obtained by

$$MDL = 20\log_{10}\left(\frac{\lambda_{\max}}{\lambda_{\min}}\right) \tag{3}$$

where λ_{max} and λ_{min} are maximum and minimum singular values of $\boldsymbol{T}$ obtained by singular value decomposition.

Here, we define three mode groups: LP_{01}, LP_{11} (LP_{11a} and LP_{11b}), and LP_{21} (LP_{21a}, LP_{21b}, and LP_{02}) mode groups. Since the modes in each mode group are easily and randomly coupled in FMF transmission, it is reasonable to consider mode-group characteristics. Figure 6 (a) and (b) show the calculated mode-group coupling matrices of G1 and G2 with taper waveguides. Figure 5 (a) an (b) are reduced to 3×3 matrices. (LP_{01}-LP_{11} and

LP_{11}-LP_{21}) conversions for G1, and (LP_{01}-LP_{21}) conversion for G2, are seen. In this paper, we call these mode-group conversions as mode-group scrambling.

2.3 Mode scrambling table and system MDL

By using these two LPGs, we propose the six-mode scrambler by cascading G2 and G1 as shown in Fig. 1 (c). Figure 7 shows the expected mode conversion process. The short taper, G2, G1, and the adiabatic taper designed above are cascaded. In the short taper, LP_{21b} and LP_{02} modes from FMF are converted to the mixture of E_{31} and E_{13} modes. In G1 and G2, five modes (except for E_{13} mode) are mixed as shown. Finally, in the adiabatic taper waveguide, E_{13} and E_{31} modes are independently converted to LP_{21b}- and LP_{02}-like modes. Figure 8 (a) and (b) show the 6×6 and 3×3 calculated mode-group coupling matrix of this device. Expected mode-group scrambling operation (LP_{01}-LP_{21}, LP_{11}-LP_{01}, and LP_{21}-LP_{11}) can be seen and the calculated MDL[21] of the device is 2.8 dB.

Although a perfectly cyclic conversion of six modes is not achieved in this configuration, multiple mode scrambling operations at the multiple relay points equalize the MDL and DMD in FMF, leading to reduced MDL in total, even if the device has finite MDL. To show the MDL reduction, we perform simple FMF transmission simulation. For the FMF, we consider 6-mode FMF and the losses of LP_{01}, LP_{11a}, LP_{11b}, LP_{21a}, LP_{21b}, and LP_{02} modes are assumed to be 0.15, 0.18, 0.18, 0.2, 0.2, and 0.23 dB/km. Here, we assume the loss of LP_{02} mode is maximum and the value is taken from [22]. Also, we assume that the loss of LP_{01} mode is similar to that of SMF. The losses of other modes are placed between them. Figure 9 (a) shows the schematic of the simulation. We consider 150-km fiber and dividing it into $N + 1$ sections when N mode scramblers are placed between two FMFs. The transmission matrices of each section are multiplied, and the MDL is calculated from the transmission matrix of the whole system. Figure 9 (b) shows the MDL of the system as a function of the number of exchanging points. Without the exchanging operation, the MDL of the system is 12 dB, corresponding to the loss difference of LP_{01} and LP_{02} modes after 150-km transmission. By increasing the number of exchanging operations, the MDL is decreased to 7 dB for $N = 2$ and 3. For $N \geq 4$, the MDL is increased again. Since the G1 and G2 have finite MDL as shown in section 2.2, the MDL of the grating becomes dominant for large number of N. Therefore, there is an optimum number for the mode

exchanging operation and it depends on the system configuration. The results indicate that, without perfectly cyclic conversion, MDL reduction is possible by proposed mode-group-scrambling based on simple cascaded LPGs with only sidewall gratings.

3. Experimental results and discussion

3.1 Loss spectra

We fabricated the designed G1 and G2 with tapered waveguides. The grating waveguides were fabricated with standard silica waveguide processing techniques. Photolithography was used to define waveguide patterns and silica is dry-etched. Then, the cladding silica was evaporated to bury the waveguide core. The six mode FMFs[23] were pigtailed and a PLC module was fabricated. First, we measured loss spectra of the module. Figure 10 shows the measurement setup. Commercially available 6 mode multiplexer (MUX) from CaiLab[24] is used to launch one of the six modes. The launched mode is transmitted in pigtailed FMF and coupled to PLC chip. The output light from the chip propagates in FMF, and demultiplexed by the 6 mode MUX. The received power is measured by an optical power meter. The received power without PLC chip is used as the reference power and subtracted. In this measurement, we cannot launch each mode to the PLC chip, because the mode is mixed in the pigtailed FMF in the same mode group. Therefore, we measured the received power of all the modes in the same mode group and take the average of them. In other words, we measured the loss of each mode group. Figure 11 (a) shows the measured loss spectra of G1. For G1, the losses of LP_{01}, LP_{11}, and LP_{21} mode group around 1.55 μm are -1.8, -3.5, and -5.3 dB. These values are larger than those of calculated. To investigate the origin of losses, we calculate the coupling efficiency between pigtailed FMF[23] and input waveguide of PLC chip (10 μm square waveguide). The calculated coupling losses per facet are -0.37, -1.25, -1.25, -2.09, -2.60, and -2.62 dB for LP_{01}, LP_{11a}, LP_{11b}, LP_{21a}, LP_{21b}, and LP_{02} mode inputs. In G1, for LP_{01} input, the loss of the input side facet is -0.37 dB. LP01 mode is converted to LP_{11a} mode in G1 and the loss at the output facet is -1.25 dB. The total loss from the face is -1.62 dB. Similarly, for LP_{11} mode group input, the loss from input facet is -1.25 dB. In G1, the LP_{11a} and LP_{11b} modes are converted to LP_{01} and LP_{21a} modes and their losses at the output facet are -0.37 and -2.09 dB. Therefore, the average loss of the output facet is -1.23 dB and the total loss from the both facets is -2.48 dB. For LP_{21} mode group input, the

average loss from input facet is – 2.44 dB. In G1, the LP_{21a} mode is converted to LP_{11b} mode and LP_{21b} and LP_{02} modes are converted to LP_{21b} and LP_{02} modes. The average loss for the output facet is -2.16 dB and the total loss from the both facets is -4.6 dB. These loss values are comparable to the measure ones and the majority of the loss seems to come from the mode field mismatch between pigtailed FMF and the square waveguide in the PLC chip. The loss can be reduced by properly designing the fiber parameters of FMF.

Figure 11 (b) shows the measured loss spectra of G2. For LP_{01} input, the loss peak can be seen around 1560 nm. For LP_{01} input, the LP_{01} mode is converted to LP_{02} mode and the losses from input and output facets are -0.37 and -2.62 dB. The total loss from both facets is about -3 dB and the value is comparable to the measured values around 1560 nm. Therefore, (LP_{01}-LP_{02}) mode conversion seems to be achieved around 1560 nm.

3.2 Mode-group exchanging characteristics

Here, we measured mode-scrambling characteristics of the modules. The experimental setup is the same as Fig. 9. We measured the output powers from all the output port of demultiplexer (DMUX) for given input and summed over the same mode group. For example, for LP_{01} input, the outputs from LP_{11a} and LP_{11b} ports are summed and the values is used as the output of LP_{11} mode group. Figure 12 (a), (b), and (c) show the measured mode-group-output of G1 for LP_{01}, LP_{11}, and LP_{21} inputs. For LP_{01} input, a clear modal conversion to LP_{11} mode group conversion can be seen. The conversion peak seems to be shifted around 1570 nm, probably due to fabrication imperfection. The modal conversion efficiency to LP_{01} mode is about 8 dB around 1570 nm. It should be noted that as explained in 3.1, these results include the mode-dependent facet loss. Therefore, the conversion efficiency may be better. For LP_{11} mode group input, LP_{01} and LP_{21} mode group output can also be seen. The modal conversion efficiency to LP_{11} mode is about 5 dB around 1570 nm. These values coincide with the calculated results (Fig. 6). Figure 13 (a), (b), and (c) show the measured mode-group-output of G2 for LP_{01}, LP_{11}, and LP_{21} inputs. While LP_{01}-LP_{21} mode group conversion can be seen, LP_{11} mode group is not converted as expected.

Figure 14 (a) and (b) show the measured mode-group coupling matrices of G1 and G2 (with tapered waveguides) for 1550 nm. In each row, the sum of the received mode powers

of the input mode group is set to 0 dB. (LP_{01}-LP_{11} and LP_{11}-LP_{21}) conversions for G1, and (LP_{01}-LP_{21}) conversion for G2, are seen. The measured matrices are in good agreement with theory (Fig. 6), showing the proof-of-concept mode converting operation. Darker colours for measured matrices (compared with Fig. 6) probably come from the coupling losses between FMF and PLC chip, waveguide scattering loss of the device and fabrication imperfection.

Figure 15 shows the measured near field patterns (NFPs) of the G1 and G2 module together with the input field NFPs. The input NFPs are taken at A point in Fig. 10, at the output of mode MUX. The output NFPs are taken at B point in Fig. 10, at the output of PLC module. It should be noted that degenerate and nearly degenerate modes in FMF (LP_{11a} and LP_{11b}, LP_{11a}, LP_{11b}, and LP_{02}) are easily mixed and cannot maintain its mode shape. Therefore, we can obtain only limited information from these NFPs. Among them, the output NFPs for LP_{01} input are more reliable because the mode shape is not change in the input FMF. For G1, Input LP_{01} mode is converted to a mode with nearly two peaks, showing the conversion to LP_{11} mode group. When LP_{11a} mode is launched, the output mode is still LP_{11}-like. This is probably due to the mode rotation in the input FMF. LP_{11b}-LP_{21a} conversion in G1 is not clear from these NFPs. This also may come from the mode rotation in FMF and the results are not inconsistent from Fig. 12 (c). For G2, input LP_{01} mode is converted to E_{31}-like mode, as expected. The output of LP_{21b} and LP_{02} inputs are E_{13}- and E_{31}-like modes. This is probably due to the waveguide width fabrication error, since the output waveguide is not square, the adiabatic taper shown in Fig. 4 (a) does not work.

4. Conclusions

The six-mode scrambler based on cascaded side-wall LPG waveguides on silica PLC platform is proposed for MDM transmission. Thanks to the careful design of the grating, two mode sets including E_{12} mode can be converted by single sidewall grating, leading to one-step etching for the fabrication. By cascading the two gratings and taper waveguides, a LP-mode-group scrambling operation, which is necessary for fiber-based MDM transmission, is possible. Fabricated gratings exhibit intended mode-group scrambling, showing the proof-of-concept. It is found that the connection between pigtailed-FMF and

PLC chip seems to be the dominant loss of the modules. By using properly designed FMF for pigtailed fiber, the loss of the module can be reduced.

References

1) R. Ryf et al., Proc of ECOC2013, 2013, We.2.D.1.
2) J. Weerdenburg et al., J. Lightwave Technol., 36, 1369 (2018).
3) T. Sakamoto et al., J. Lightwave Technol., 36, 325 (2018).
4) Y. Wakayama et al., Proc of OFC2016, 2016, M3E.6.
5) K. Shibahara et al., Proc of OFC2020, 2020, Th3H.3.
6) B.B. Oner et al., Opt. Express, 23, 3186 (2015).
7) M. Ye, Y. Yu, C. Sun, and X. Zhang, Opt. Express, 24, 528 (2016).
8) C. Sun, Y. Yu, G. Chen, and X. Zhang, Opt. Lett., 41, 3257 (2016).
9) Y. Sawada, T. Sato, T. Fujisawa, and K. Saitoh, J. Lightwave Technol., 36, 3652 (2018).
10) Y. Sawada, T. Fujisawa, and K. Saitoh, Optics Express, 28, 38196 (2020).
11) W. Jin and K.S. Chiang, Opt. Lett., 41, 3130 (2016).
12) W. Wang et al., Opt. Express, 25, 14341 (2017).
13) W. Jin and K. S. Chiang, Opt. Express, 26, 15289 (2018).
14) T. Fujisawa et al., Proc of OFC2017, 2017, W1B.2.
15) B. Huang et al., Opt. Lett., 42, 3594 (2017).
16) H. Chen et al., Proc of ECOC2017, 2017, W2F3.
17) Y. Zhao et al., Opt. Lett., 43, 2868 (2018).
18) M. Shirata et al., Proc of IEEE Photonics Conference 2019, 2019, TuH1.4.
19) Y. Yamashita et al., J. Lightwave Technol., 35, 2252 (2017).
20) K. Saitoh et al., Optical Fiber Technology, 35, 80 (2017).
21) T. Fujisawa et al., J. Lightwave Technol., 36, 1985 (2018).
22) T. Sakamoto et al., J. Lightwave Technol., 35, 443 (2017).
23) T. Mori et al., J. Lightwave Technol., 32, 2468 (2014).
24) 'Proteus', https://www.cailabs.com/en/product/proteus-s/

Figure Captions

Fig. 1. (a) Field distributions of six modes in a rectangular waveguide. (b) Mode conversion combinations for sidewall and surface gratings. (c) A schematic of proposed mode scrambler and isolated LPG waveguide.

Fig. 2. Calculated conversion spectra of G1 for (a) LP01, (b) LP21a input, and (c) G2 for LP01 mode input.

Fig. 3. $|E_x|$ field distributions in xz-plane of (a) G1 for E_{11} and E_{12} input and (b) G2 for E_{11} input.

Fig. 4. (a) Mode conversion process in short and adiabatic taper waveguides. (b) Modal output powers of short taper calculated by BPM.

Fig. 5. 6×6 Calculated mode coupling matrices of (a) G1 and (b) G2.

Fig. 6. 3×3 Calculated mode coupling matrices of (a) G1 and (b) G2.

Fig. 7. Expected mode conversion process in proposed mode scrambler.

Fig. 8. (a) 6×6 and (b) 3×3 calculated mode coupling matrix of proposed mode scrambler.

Fig. 9. (a) A schematic of FMF transmission with N mode-scrambling points. and (b) MDL as a fucntin of the number of mode-scrambling points.

Fig. 10. Measurement setup.

Fig. 11. Measured loss spectra of each mode group of (a) G1 and (b) G2.

Fig. 12. Measured mode-group output spectra of G1 for (a) LP01, (b) LP11, and (c) LP21 mode group input.

Fig. 13. Measured mode-group output spectra of G2 for (a) LP01, (b) LP11, and (c) LP21 mode group input.

Fig. 14. Measured mode coupling matrices of (a) G1, (b) G2.

Fig. 15. Measured NFPs of Input, G1, and G2.

Table I. Structural parameters of G1 and G2.

	Λ [μm]	*d* [μm]	*L* [μm]
G1	440	0.5	6160 (14 periods)
G2	170	0.5	3910 (23 periods)

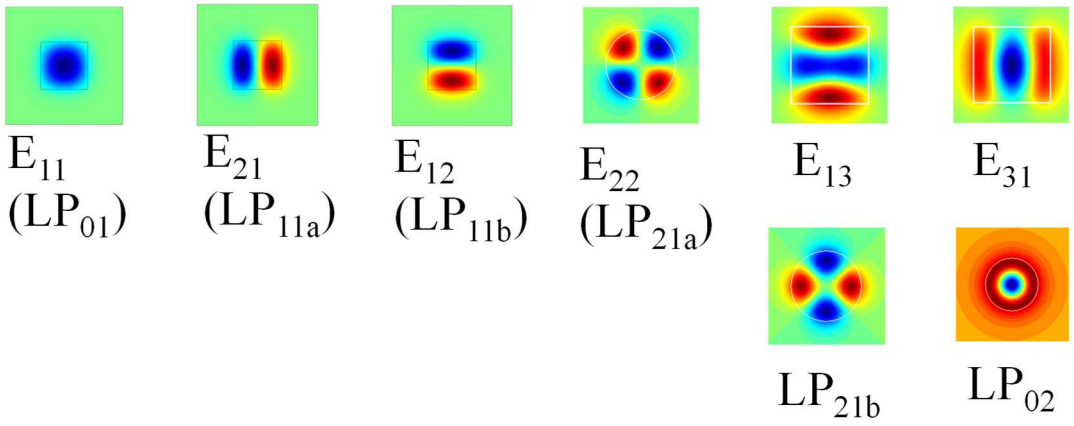
E11
(LP01)
E21
(LP11a)
E12
(LP11b)
E22
(LP21a)
E13
E31
LP21b
LP02

(a)

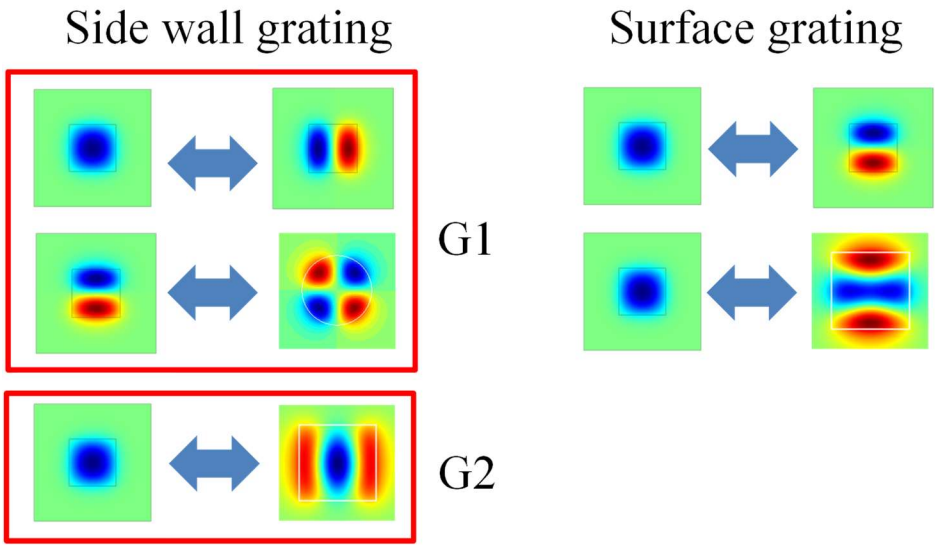
Side wall grating
Surface grating
G1
G2

(b)

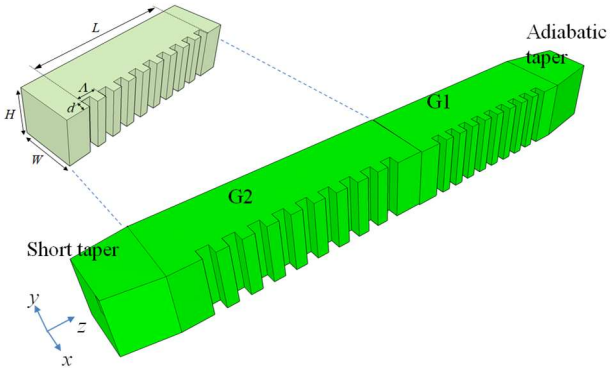
L
Λ
d
H
W
Adiabatic
taper
G1
G2
Short taper
y
z
x

(c)

Fig.1.

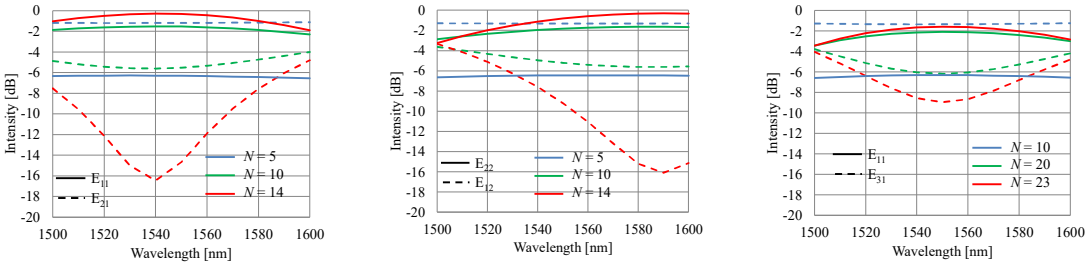

Fig. 2.

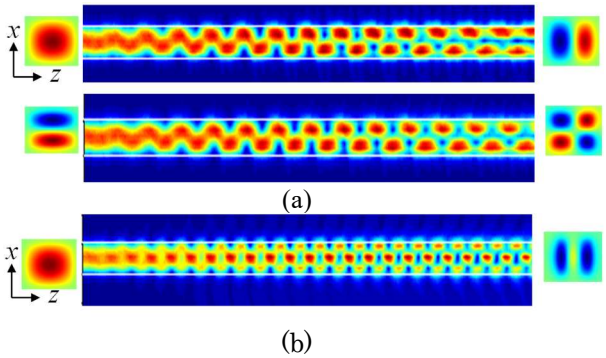

Fig. 3.

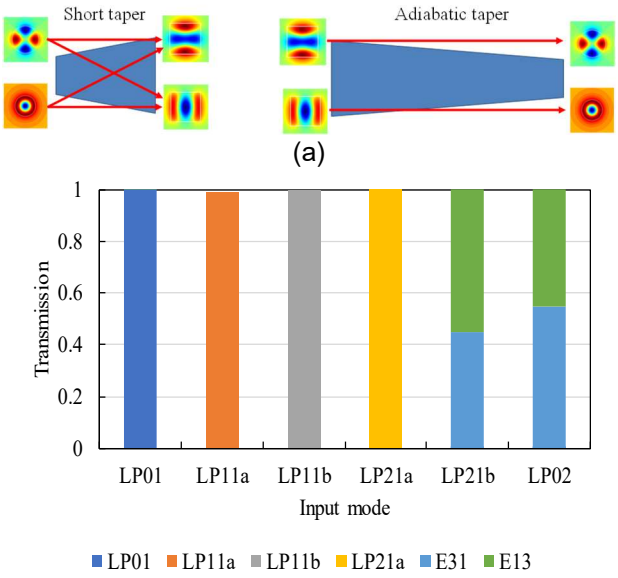

Fig. 4.

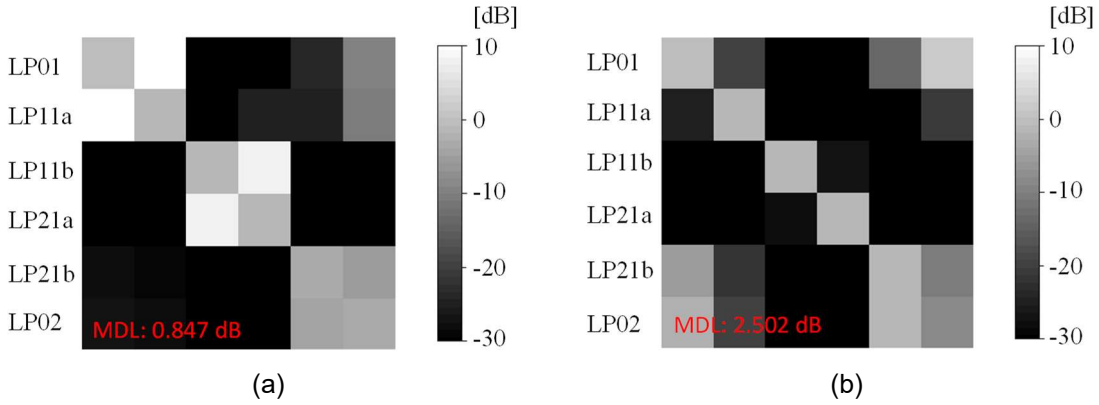
[dB]
10
0
-10
-20
-30
LP01
LP11a
LP11b
LP21a
LP21b
LP02
MDL: 0.847 dB
(a)
[dB]
10
0
-10
-20
-30
LP01
LP11a
LP11b
LP21a
LP21b
LP02
MDL: 2.502 dB
(b)

Fig. 5.

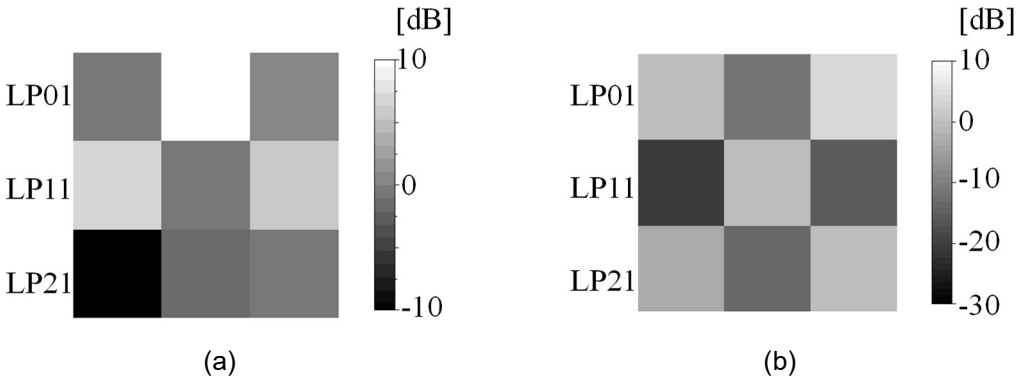
[dB]
10
0
-10
LP01
LP11
LP21
(a)
[dB]
10
0
-10
-20
-30
LP01
LP11
LP21
(b)

Fig. 6.

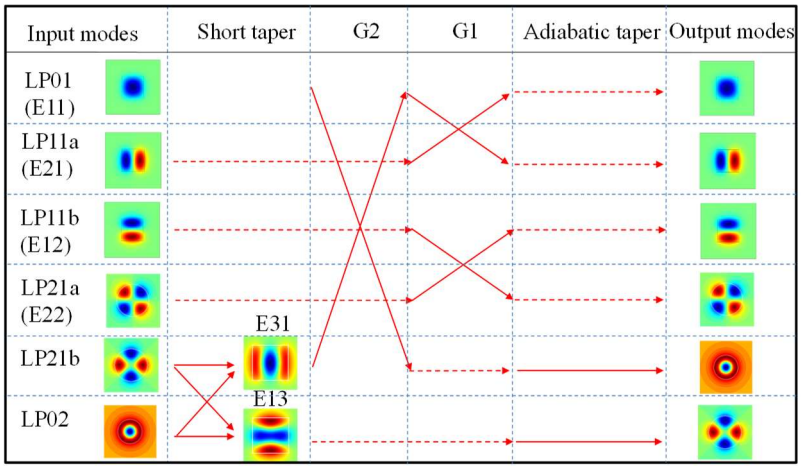
Input modes
Short taper
G2
G1
Adiabatic taper
Output modes
LP01
(E11)
LP11a
(E21)
LP11b
(E12)
LP21a
(E22)
LP21b
LP02
E31
E13

Fig. 7.

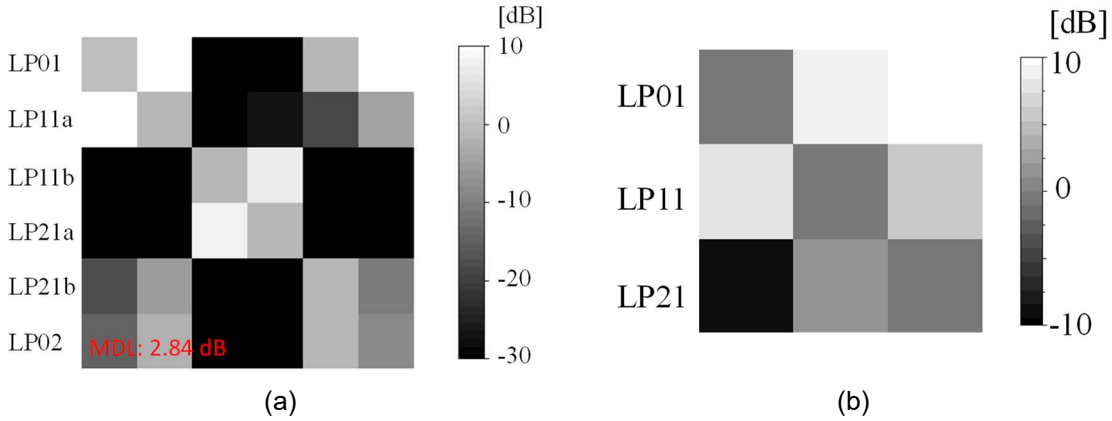

Fig. 8.

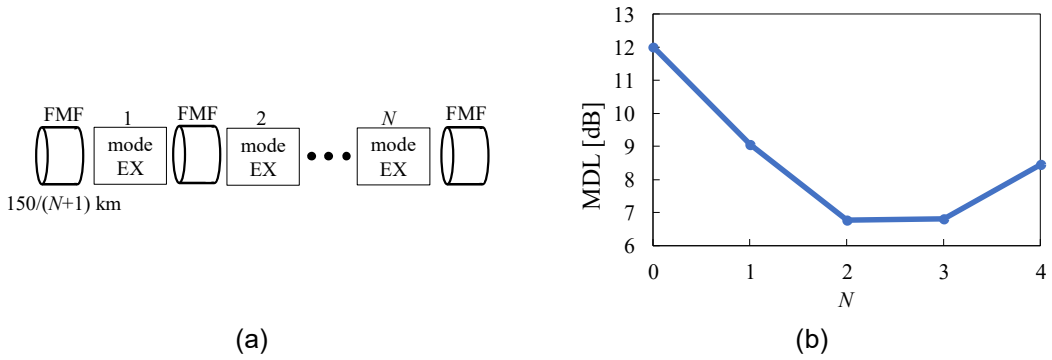

Fig. 9.

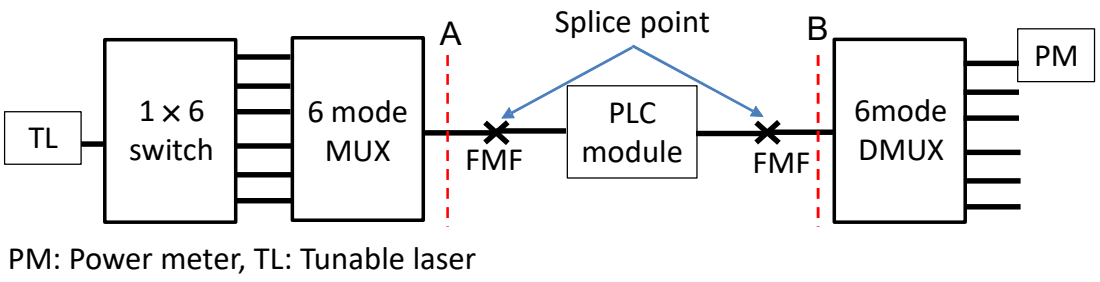

Fig. 10.

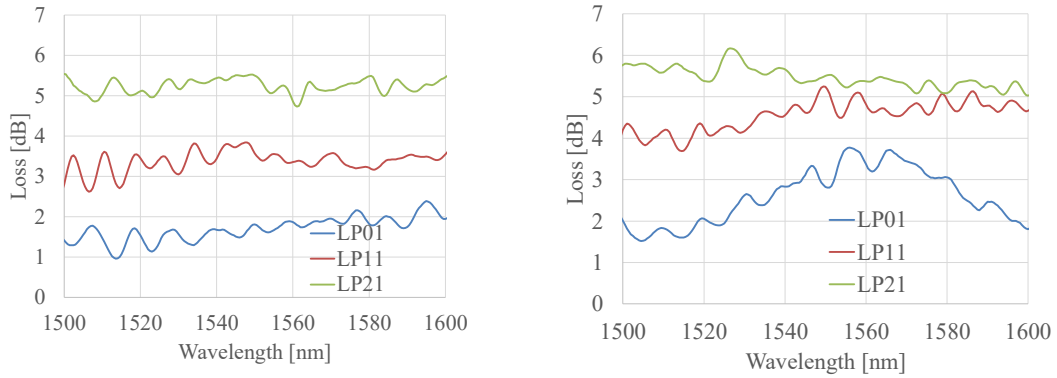

Fig. 11.

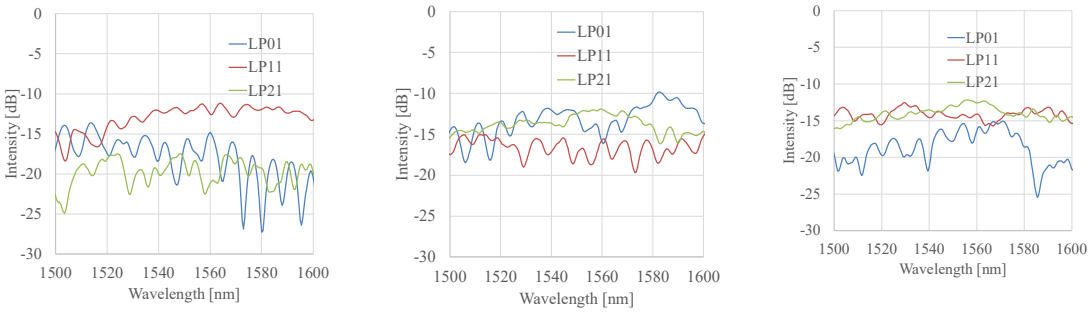

Fig. 12.

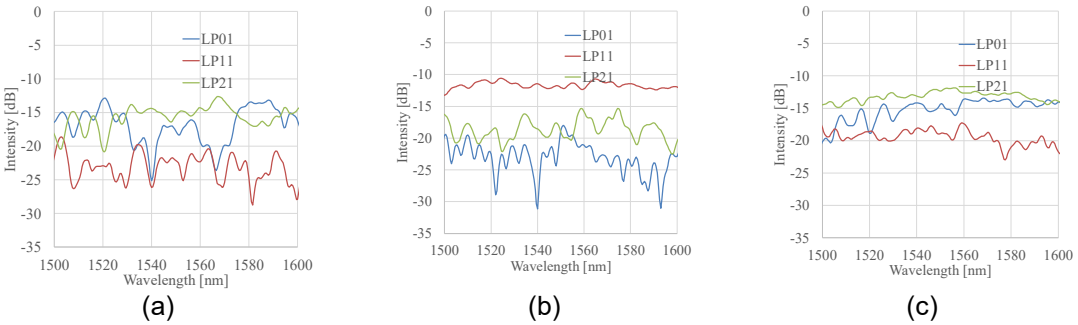

Fig. 13.

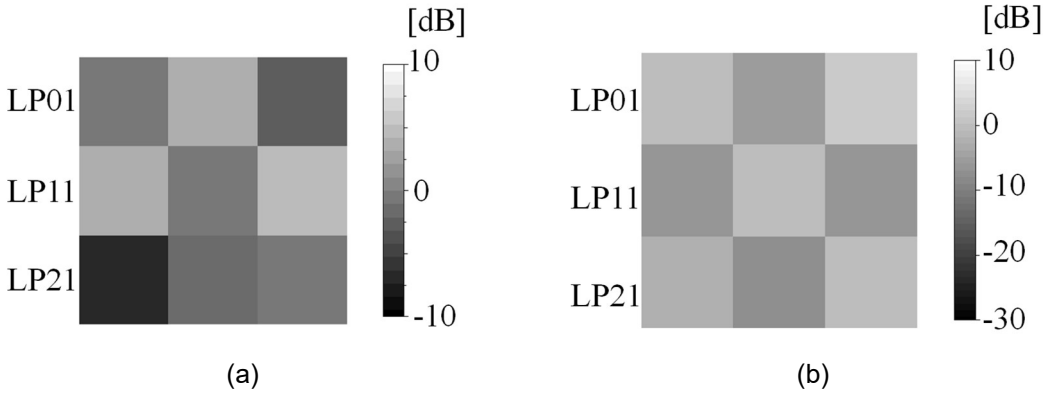
[dB]
10
0
-10
LP01
LP11
LP21
(a)
[dB]
10
0
-10
-20
-30
LP01
LP11
LP21
(b)

Fig. 14.

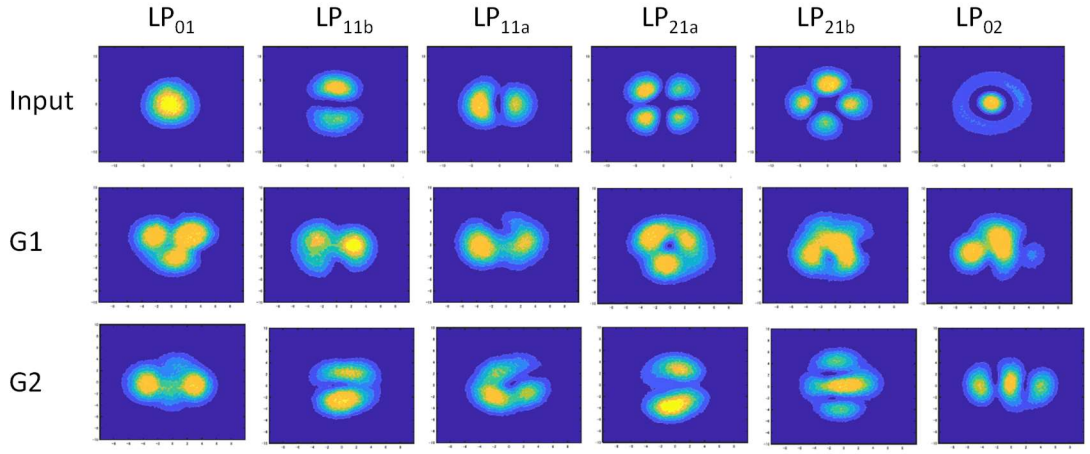
LP01
LP11b
LP11a
LP21a
LP21b
LP02
Input
G1
G2

Fig. 15.